The Role of Atlantic Heat Transport in Future Arctic Winter Sea Ice Loss

Marius Årthun, Tor Eldevik, and Lars H. Smedsrud

Geophysical Institute, University of Bergen, and Bjerknes Centre for Climate Research, Bergen, Norway

ABSTRACT

During recent decades Arctic sea ice variability and retreat during winter have largely been a result of variable ocean heat transport (OHT). Here we use the Community Earth System Model (CESM) large ensemble simulation to disentangle internally and externally forced winter Arctic sea ice variability, and to assess to what extent future winter sea ice variability and trends are driven by Atlantic heat transport. We find that OHT into the Barents Sea has been, and is at present, a major source of internal Arctic winter sea ice variability and predictability. In a warming world (RCP8.5), OHT remains a good predictor of winter sea ice variability, although the relation weakens as the sea ice retreats beyond the Barents Sea. Warm Atlantic water gradually spreads downstream from the Barents Sea and farther into the Arctic Ocean, leading to a reduced sea ice cover and substantial changes in sea ice thickness. The future long-term increase in Atlantic heat transport is carried by warmer water as the current itself is found to weaken. The externally forced weakening of the Atlantic inflow to the Barents Sea is in contrast to a strengthening of the Nordic Seas circulation, and is thus not directly related to a slowdown of the Atlantic meridional overturning circulation (AMOC). The weakened Barents Sea inflow rather results from regional atmospheric circulation trends acting to change the relative strength of Atlantic water pathways into the Arctic. Internal OHT variability is associated with both upstream ocean circulation changes, including AMOC, and large-scale atmospheric circulation anomalies reminiscent of the Arctic Oscillation.

1. Introduction

The Arctic Ocean (Fig. 1) is currently losing sea ice in all regions during all seasons (Serreze et al. 2007; Cavalieri and Parkinson 2012; Stroeve et al. 2012; Onarheim et al. 2018). These changes in the Arctic sea ice cover could potentially have both local and remote impacts on the climate system, influencing the surface energy budget (Bhatt et al. 2014; Lee et al. 2017), oceanic (Krishfield et al. 2014; Sévellec et al. 2017) and atmospheric (Vihma 2014; Screen 2017; Ogawa et al. 2018) circulation patterns, and marine ecosystems (Arrigo and van Dijken 2011; Årthun et al. 2018) and mammals (Kovacs et al. 2011). A better understanding of the future evolution of Arctic sea ice and its drivers is therefore essential. Here, we focus on sea ice retreat in winter, which so far has received less attention than the more dramatic summer sea ice decline, but which is expected to become more dominant as the Arctic transitions toward an ice-free summer (Onarheim et al. 2018).

In winter, recent Arctic sea ice loss has been most pronounced in the Barents Sea (Li et al. 2017; Onarheim and Årthun 2017). The retreating sea ice has largely been a result of ocean heat transport changes associated with the Norwegian Atlantic Current, the northernmost extension of the Gulf Stream (Fig. 1) (Francis and Hunter 2007; Årthun et al. 2012; Smedsrud et al. 2013; Li et al. 2017). Future projections show a continued reduction of the winter sea ice cover in the Arctic Ocean as a response to greenhouse gas emissions, although with a large spread (uncertainty) in projected trends as a result of model differences and internal climate variability (Overland and Wang 2007; Hodson et al. 2013; Sandø et al. 2014; Barnhart et al. 2016; Long and Perrie 2017; Onarheim and Årthun 2017). On interannual to decadal time scales, internal variability in, for example, poleward ocean heat transport can lead to

---

ⓞ Denotes content that is immediately available upon publication as open access.

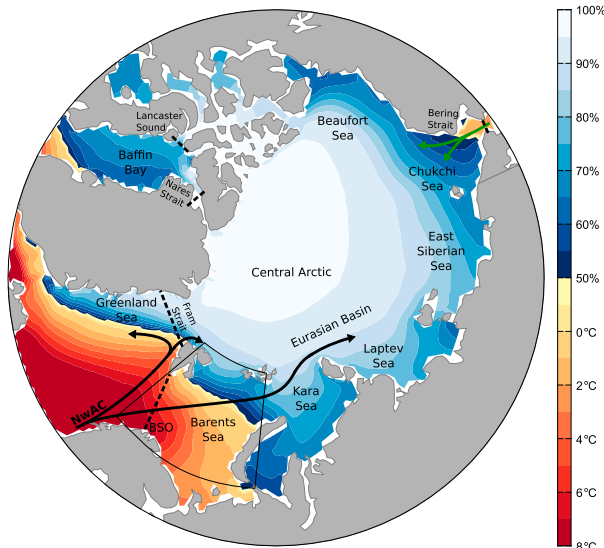*Corresponding author*: Marius Årthun, marius.arthun@uib.no

FIG. 1. The Arctic Ocean and its marginal seas. Colors show annual mean sea ice concentration and sea surface temperature in CESM-LE for 2010–19 (ensemble mean). The black arrows show the main pathways of Atlantic water toward the Arctic Ocean (NwAC: Norwegian Atlantic Current) and the green arrows denote the inflow of Pacific water through the Bering Strait. The black dashed lines indicate sections through which heat transports are calculated; between Norway and Svalbard (Barents Sea Opening; BSO), across the Fram Strait, Bering Strait, Nares Strait, and Lancaster Sound. The Barents Sea is defined by the thin black lines.

intermittent recoveries of the sea ice cover, superimposed on the long-term decline (Yeager et al. 2015; Zhang 2015; Årthun et al. 2017; Onarheim and Årthun 2017). Conversely, pulses of ocean heat can also lead to abrupt Arctic sea ice loss (Holland et al. 2006). To understand and possibly constrain how the Arctic winter sea ice cover will evolve in the future it is therefore important to ascertain to what extent future Arctic sea ice variability and retreat are influenced by internal variability of the Atlantic inflow. We furthermore investigate to what extent the loss of winter sea ice will progress beyond the Barents Sea, deeper into the Arctic, as a response to a poleward expansion of Atlantic waters.

The relationship between ocean heat transport and sea ice anomalies has furthermore allowed for skillful predictions of the winter Arctic sea ice cover on interannual (Nakanowatari et al. 2014; Onarheim et al. 2015) and multiannual time scales (Yeager et al. 2015; Årthun et al. 2017). However, the importance of atmospheric conditions has been suggested to increase as the sea ice retreats (Smedsrud et al. 2013). Interannual predictability of Arctic summer sea ice has been found to decrease as it retreats in the future (Holland et al. 2011; Tietsche et al. 2013), and predictor relationships

change between present-day and future climate simulations (Holland and Stroeve 2011). An important, and yet unresolved, question is therefore to what extent the predictable relationship between ocean heat transport and sea ice changes in a warming climate.

To investigate the importance of ocean heat transport for future Arctic sea ice loss, and to disentangle the relative roles of internally and externally forced climate variability, we use the Community Earth System Model large ensemble simulation (CESM-LE; Kay et al. 2015). The CESM-LE has previously been used to assess the influence of internal variability on Arctic summer sea ice trends (Swart et al. 2015; Barnhart et al. 2016; Jahn et al. 2016). The analysis is structured as follows. First, we assess the ability of the CESM-LE to represent present-day ice–ocean interaction in the Barents Sea (section 3). Then, we examine the importance of internal variability in Arctic sea ice variability and trends (section 4), and the role of ocean heat transport as a driver of the internal sea ice variability (section 5). Finally, in light of the recent "Atlantification" of the Arctic Ocean (Årthun et al. 2012; Polyakov et al. 2017), we address the drivers of future changes in poleward ocean heat transport (section 6) and the implications for the hydrography in the downstream Eurasian basin (section 7).

2. Data and methods

a. CESM-LE

To assess future Arctic climate variability we use data from the large ensemble simulation by the Community Earth System Model (CESM-LE; Kay et al. 2015). The fully coupled CESM1 model consists of the Community Atmosphere Model version 5; the Parallel Ocean Program, version 2 (POP2); the Community Land Model, version 4; and the Community Ice Code, version 4 (CICE4) (Hurrell et al. 2013). The spatial resolution of the CESM ocean and sea ice models is nominally 1° longitude by latitude, whereas the atmospheric model is 0.9° × 1.25°.

The CESM-LE includes 40 ensemble members for the time period 1920 to 2100. Here we mainly use data until 2080, because by then the Barents Sea, which is an area of particular interest, is practically ice-free (Fig. 2a; Onarheim and Årthun 2017). The CESM-LE simulations start from an 1850 constant forcing control simulation (Kay et al. 2015). The first ensemble member is initialized from a randomly selected year (1 January, year 402) of the control simulation, and integrated forward from 1850 to 2100 using historical forcing for the period 1920–2005 and representative concentration pathway (RCP) 8.5 forcing from 2006 to 2100 (Taylor et al. 2012). The
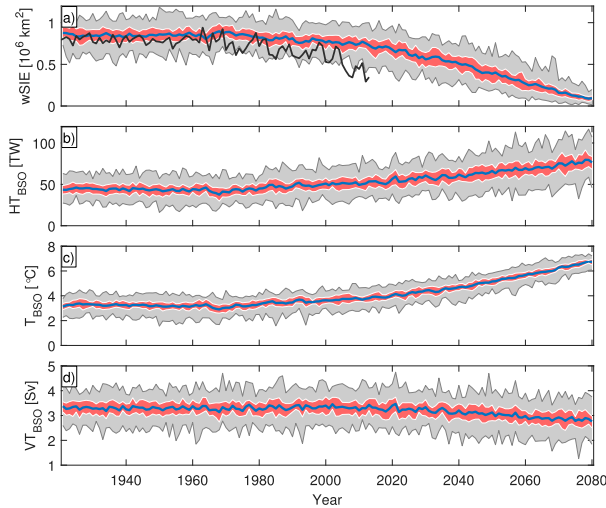
FIG. 2. Time series of (a) winter sea ice extent (wSIE) in the Barents Sea, (b) heat transport through the BSO (HT$_{BSO}$), (c) average temperature (T_{BSO}), and (d) volume transport of the BSO inflow (VT$_{BSO}$). Blue line: ensemble mean; red shading: interquartile range; gray shading: ensemble spread. The black line in (a) shows the observation-based winter sea ice extent from Walsh et al. (2017).

remaining ensemble members are then started in 1920 using initial conditions from the first ensemble member, but with random round-off level differences in the initial air temperature fields. As the ensemble members all use the same Earth system model and the same external forcing, the ensemble spread is thus only generated by simulated internal climate variability originating from the very small differences in the initial conditions of each member.

b. Ocean heat and volume transport

Ocean heat transport (OHT) across a section is defined as

$$OHT = \rho c_p \int_S \mathbf{U}(T - T_{ref})dS, \qquad (1)$$

where ρ and c_p are constant density and specific heat, respectively, $\mathbf{U}$ is the velocity perpendicular to the section, T is the temperature, and S is the surface area of the section. Here OHT is calculated as the spatial integral of the advective heat flux (model variables UET and VNT) normal to the gridcell faces. Similarly, volume transport is calculated using the vertically integrated velocities (variables SU and SV). As the volume transport across individual sections is not balanced, the heat transport calculation depends on the arbitrary reference temperature T_{ref} (Schauer and Beszczynska-Möller 2009). In CESM-LE $T_{ref} = 0°C$ is used, which enables comparison with previous heat transport estimates from the Barents

Sea Opening (BSO; e.g., Årthun et al. 2012; Smedsrud et al. 2013; Koenigk and Brodeau 2014; Li et al. 2017).

We here focus on Atlantic heat transport through the BSO (Fig. 1) as this is the largest contributor of oceanic heat to the Arctic (Beszczynska-Möller et al. 2011; Rudels et al. 2015). Atlantic water also enters the Arctic Ocean via the Fram Strait. In CESM-LE the average net heat transport in this branch (calculated across 79°N for 2006–80) is approximately 25% of that in the BSO branch (30% if considering only the northward flowing water), although we note that coarse-resolution climate models most likely underestimate transport through the Fram Strait (Ilıcak et al. 2016). The non-Atlantic heat exchanges to the Arctic—between the Pacific Ocean and Arctic Ocean through the Bering Strait, and across the Canadian polar shelf through the Nares Strait and Lancaster Sound (Fig. 1)—are also small compared with the BSO.

In agreement with observations (Årthun et al. 2012), the simulated BSO heat transport has a well-defined seasonal cycle with a minimum in spring (May), followed by a gradual increase toward an early winter maximum (November; not shown). Heat transport is therefore presented as winter-centered annual averages, defined as July of the previous year through June of the named year.

To assess whether variable ocean heat transport into the Arctic is related to large-scale ocean circulation changes in the North Atlantic, we also calculate the strength of the Atlantic meridional overturning circulation (AMOC). AMOC strength is defined as the maximum of the zonally integrated meridional overturning streamfunction (model variable MOC) in the Atlantic basin. We here consider the traditional AMOC index at 26°N, but similar results are obtained for a more northern AMOC (50°N).

c. Sea ice extent

The Arctic winter (November–April) sea ice extent (wSIE) is calculated as the total area of all the grid cells where the sea ice concentration exceeds 15%. The Barents Sea includes the area 70°–81°N, 15°–60°E (Fig. 1).

d. Statistical methods

A main aim of this paper is to disentangle the role of external and internal variability in Arctic winter sea ice retreat. The externally forced response is obtained by averaging all ensemble members, and the internally generated variability is then the total variability minus the externally forced component. The relative importance of internal variability and external forcing in driving wSIE trends is quantified by calculating the

signal-to-noise ratio (SNR). The SNR is defined as the absolute value of the externally forced trend divided by the standard deviation of trends across the individual ensemble members (Deser et al. 2014). An SNR value greater than 1 implies that the impact of the external forcing is stronger than the internal variability.

To assess the relationship between internally driven trends in OHT and sea ice we regress the BSO heat transport trend from the individual ensemble members onto the wSIE. This is referred to as ensemble trend regression (Wettstein and Deser 2014). When discussing temporal changes in the sea ice cover we mainly consider 30-yr trends (cf. Serreze and Stroeve 2015). To highlight any future differences in ice–ocean interaction, we specifically compare the historical period 1976–2005 with the two future periods, 2031–60 and 2051–80, representing mid- and late-century conditions, respectively.

3. Simulated ice–ocean interaction and trends in present climate

We first evaluate the ability of CESM-LE to simulate present-day ice–ocean interaction, focusing on the Barents Sea where long-term observations of OHT are available (Årthun et al. 2012). The ensemble mean heat transport through the BSO during the last decade (2000–15) is 55 TW (Fig. 2b; $1\,\mathrm{TW} \equiv 10^{12}\,\mathrm{J\,s^{-1}}$), with an ensemble standard deviation of 8 TW (Fig. 2b). The observational estimate is 70 ± 5 TW (Smedsrud et al. 2013). The underestimated BSO heat transport in CESM-LE can be explained by lower temperatures than observed; a comparison with observed sea surface temperatures (HadISST; Rayner et al. 2003) reveals a cold temperature bias in the Barents Sea (not shown). The lower temperatures are furthermore reflected in an overestimated sea ice cover, especially during recent decades (Fig. 2a; Park et al. 2014). The simulated volume transport through the BSO is, on the other hand, higher than observed (3.0 Sv in CESM vs 2.3 Sv in observations; Smedsrud et al. 2013). We note that although the observations do not cover the full BSO as defined here (Fig. 1), only the southern part between 71.5° and 73.5°N (Ingvaldsen et al. 2004), this is not a major source of discrepancy as the simulated flow in the northern part of the section is weak.

In agreement with observations, the relationship between OHT and wSIE for the recent past (1976–2005) is strong for both interannual variability (comparing standard deviations) and the long-term trend (Fig. 3a,d). The results are similar if we consider the full historical time period (1920–2005). The sensitivity of simulated sea ice extent to interannual heat transport variations is also consistent with observations. The regression slope translates into a wSIE change of $90 \times 10^3\,\mathrm{km^2}$ per 10 TW of anomalous OHT (Fig. 3a), which is slightly larger than the observation based sensitivity of $70 \times 10^3\,\mathrm{km^2}$ per 10 TW (Årthun et al. 2012).

Although a detailed evaluation of Arctic–Atlantic ice and ocean properties in CESM is not performed here, the model appears to realistically simulate the present-day inflow of Atlantic heat to the Barents Sea and the associated response in sea ice cover, providing confidence in the model's ability to assess future changes. CESM-LE has also previously been used to study Arctic sea ice change (e.g., Swart et al. 2015; Barnhart et al. 2016; Jahn et al. 2016; Labe et al. 2018).

4. The importance of internal variability for Arctic winter sea ice loss

The spatial patterns of Arctic winter sea ice concentration trends are shown in Fig. 4. For the historical period, the largest ensemble mean trends generally occur in the central Barents Sea and Greenland Sea (Fig. 4a). The internal variability, expressed as the standard deviation of trends across the ensemble members, shows a similar pattern (Fig. 4d). Except for large parts of the central Arctic the magnitude of internal variability is larger than external variability, and, as a consequence, the signal-to-noise ratio shows values < 1 (Fig. 4g). The magnitude and importance of internal variability in the Barents Sea are also evident from the range in wSIE trends across the ensemble members, with some members even showing increased SIE between 1976 and 2005 (Fig. 3d).

In contrast the externally forced signal becomes the dominant factor for sea ice loss in the future (Figs. 4h,i). Externally forced sea ice loss is especially pronounced in the central Arctic Ocean. For the Barents Sea, positive 30-yr trends no longer occur (Figs. 3e,f), which implies that internal variability is not strong enough to counteract the externally forced sea ice loss for any ensemble member. This is, however, for the total Barents Sea ice extent. Locally, there is still a 20%–30% chance for the sea ice concentration to increase in the southeastern Barents Sea between 2031 and 2060 (Fig. 5a; quantified as the number of ensemble members with positive trends divided by the total number of ensemble members; Deser et al. 2014). We note that internal variability in the North Atlantic Ocean is underestimated in CESM-LE (Kim et al. 2018), implying that the occurrence and strength of internally generated trends in Arctic winter sea ice, as calculated here, might also be underestimated. The CESM-LE simulations furthermore use the strong
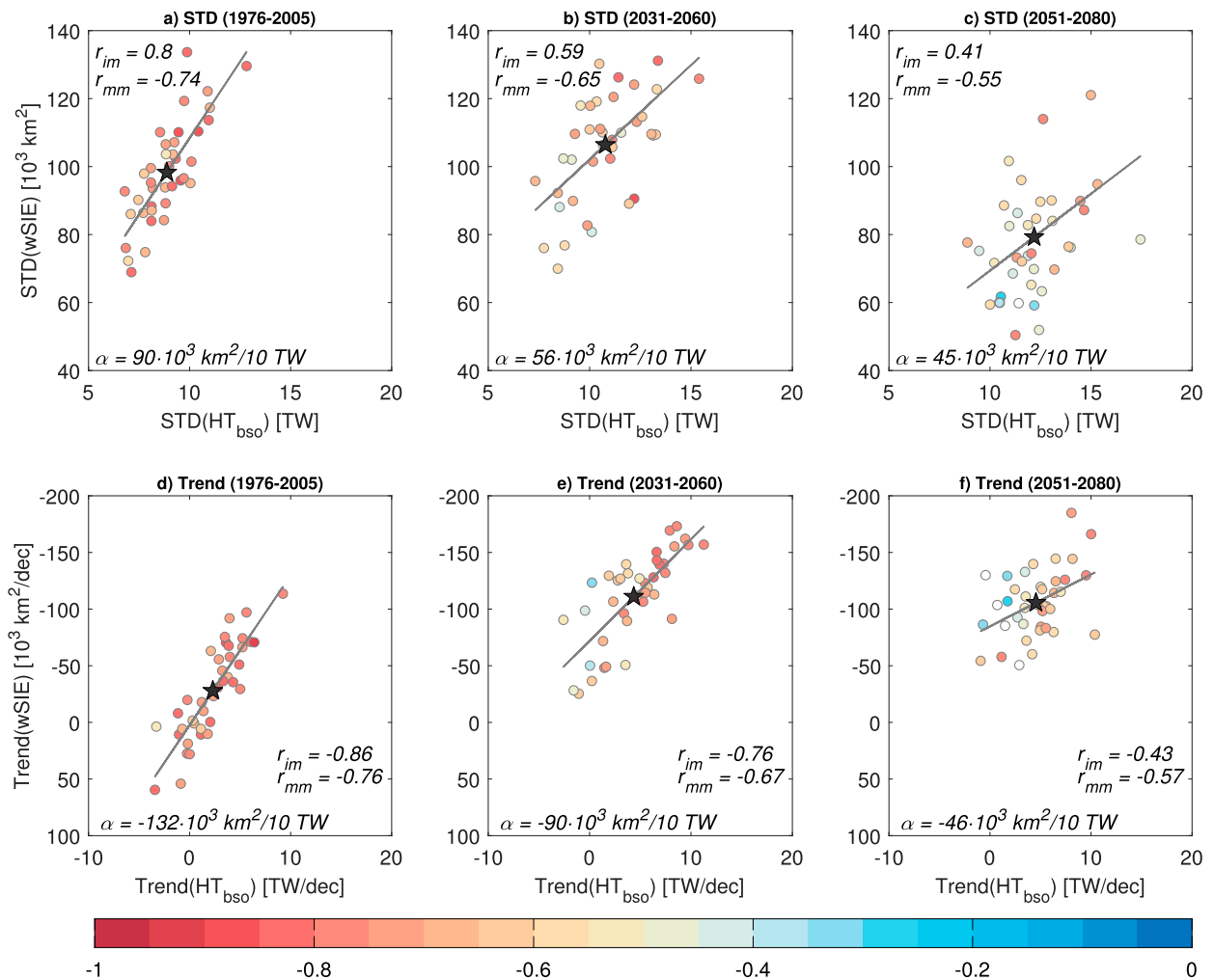
FIG. 3. The relationship between winter sea ice extent in the Barents Sea and BSO heat transport for a historical time period (1976–2005) and in the future (2031–60 and 2051–80), considering interannual variability (comparing standard deviations; STD) and the long-term linear trend. Colors show correlation between winter sea ice extent (wSIE) and ocean heat transport for (a)–(c) detrended and (d)–(f) full time series. White circles indicate correlations not significant at the 95% confidence level (Ebisuzaki 1997). The black stars show the ensemble mean. Multimember average correlation (r_{mm}; average correlation across ensemble members) and intermember correlation (r_{im}; relationship between ensemble members) coefficients are provided. Linear regression lines are shown by solid lines, and their slope α is provided.

forcing scenario RCP8.5 and therefore, by construction, have a strong externally forced signal. These considerations suggest that the SNR computed from CESM-LE is an upper bound.

The relative importance of internal and external variability is also highly dependent on the trend length considered (Fig. 6; Kay et al. 2011; Swart et al. 2015). The SNR increases with increasing trend length, and for the time period 2007–80 external variability dominates multidecadal ($\geq$20 yr) winter sea ice trends in the Barents Sea. The time scale at which external variability becomes dominant is increased (decreased) if we consider the early (later) part of the time series

(corresponding to the error bars in Fig. 6). However, on decadal time scales the signal-to-noise ratio in the Barents Sea is < 1 also in the future. Hence, future interannual to decadal-scale wSIE variability and trends in the Barents Sea are still expected to be dominated by internal variability. This is further evidenced by positive 10-yr trends still occurring frequently between 2031 and 2040 (Fig. 5b); the chances of sea ice expansion during this decade is 40%–50% in the southeastern Barents Sea. The chance of positive decadal trends is also high in the other Arctic shelf seas and in the Greenland Sea. Similar values are obtained if we consider other future 10-yr periods. Next we assess to what extent these internal
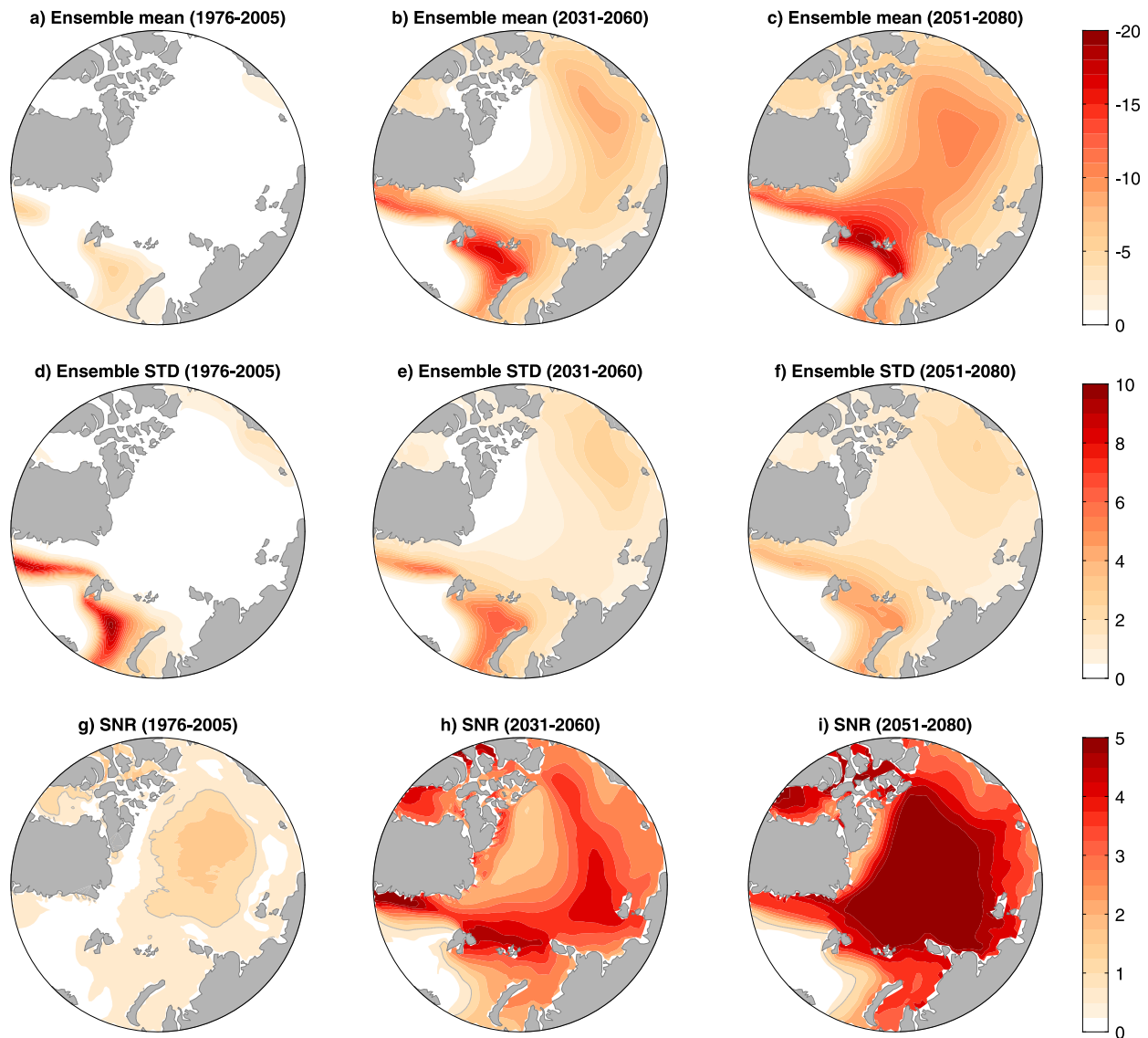
FIG. 4. (a)–(c) Ensemble mean winter sea ice concentration trend for the time periods 1976–2005, 2031–60, and 2051–80 (% decade^{-1}). (d)–(f) Ensemble standard deviation of trends. (g)–(i) Signal-to-noise ratio (SNR), defined as the absolute value of the ensemble mean (external) trend divided by the standard deviation of trends across the individual ensemble members (internal). An SNR value greater than one (gray contour) implies that the impact of the external forcing is stronger than the internal variability.

variations in Arctic sea ice loss are driven by Atlantic heat transport.

5. Atlantic heat transport as a driver of internal Arctic winter sea ice variability and trends

Ensemble trend regression reveals the extent to which internal variability in OHT trends drives trends in Arctic sea ice loss (Fig. 7). For the historical period, the regression coefficients are highest in the central Barents Sea and in the Greenland Sea, whereas for the future time periods the maximum values move northeastward

into the Kara Sea and Laptev Sea. The northeastward spread of future OHT-driven internal sea ice variability broadly corresponds to the poleward pathway of Atlantic water (Fig. 1; Rudels et al. 2015). The spatial patterns furthermore qualitatively match those found for the ensemble standard deviation of sea ice trends (Figs. 4d–f). The similarity between the spatial patterns of the ensemble spread and ensemble trend regression provides evidence that OHT is a major source of internal variability in wSIE trends. This is consistent with Li et al. (2017) who, using a suite of CMIP5 models, also found that winter sea ice loss in the Barents Sea during
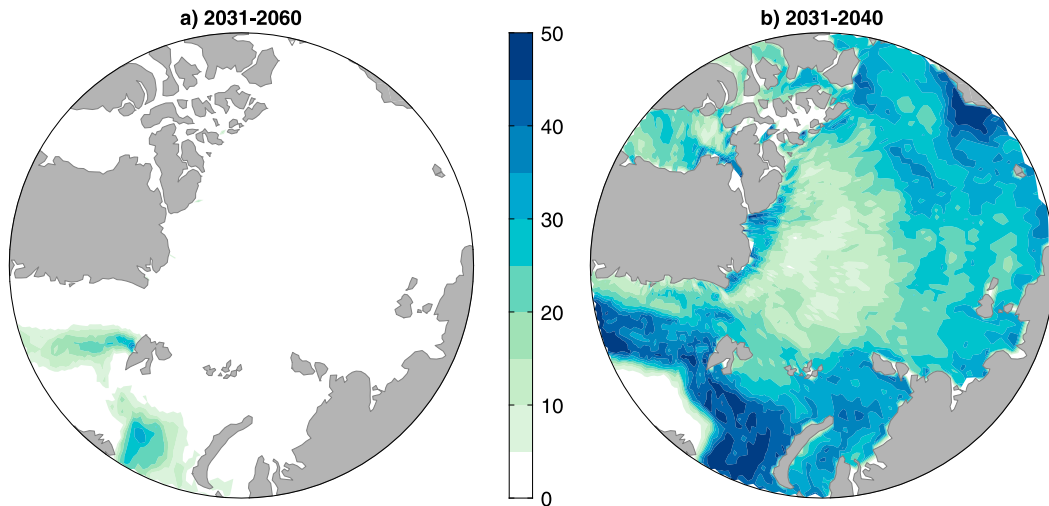
FIG. 5. Chance (in %) of a positive trend (expansion) in sea ice cover over the periods (a) 2031–60 and (b) 2031–40, quantified as the number of ensemble members with positive trends divided by the total number of ensemble members.

recent decades predominately has been a result of internal heat transport variability.

Since it is a major source of present-day Arctic winter sea ice predictability, and in the Barents Sea in particular (Onarheim et al. 2015), we next assess whether the strength of the relationship between ocean heat transport and winter sea ice extent is expected to change in the future. Considering the period 2031–60, the strong relationship between wSIE and OHT persists, although both the multimember and intermember correlations weaken compared with 1976–2005 (Figs. 3b,e). As the Barents Sea starts becoming perennially ice free (Fig. 2a) the link to OHT continues to weaken, both in terms of interannual variability and trends (2051–80; Figs. 3c,f). For this latter part of the century, changes in sea ice area, both interannual (comparing standard deviations) and the long-term trend, have been reduced to about 45 × 10^3 km^2 retreat with 10 TW of additional heat.

To further assess whether the OHT–wSIE relationship is stationary throughout the full time series (1920–2080), the correlation between detrended wSIE and OHT is calculated for overlapping 30-yr periods for each ensemble member (Fig. 8). Consistent with that seen in Fig. 3 (r_{mm}) and Fig. 7 the relationship persists throughout most of the period, although the mean correlation across the ensemble members weakens toward the end of the time series as the sea ice retreats (Fig. 2a). Note, however, that the correlation between OHT and wSIE for individual ensemble members is not simply a function of the mean sea ice extent. That is, the ensemble members with a relatively small sea ice extent toward the end of the time series period are not necessarily those with the lowest correlations with

OHT. The generally weakened correlation is consistent with Smedsrud et al. (2013), who argued, based on a simple conceptual heat budget model of the Barents Sea, that the sea ice sensitivity to oceanic forcing decreases as the sea ice retreats, and that the role of atmospheric forcing increases accordingly. The importance of atmospheric forcing on future Arctic sea ice variability and trends (e.g., Wettstein and Deser 2014; Ding et al. 2017), and whether this changes with time, is, however, not assessed here.
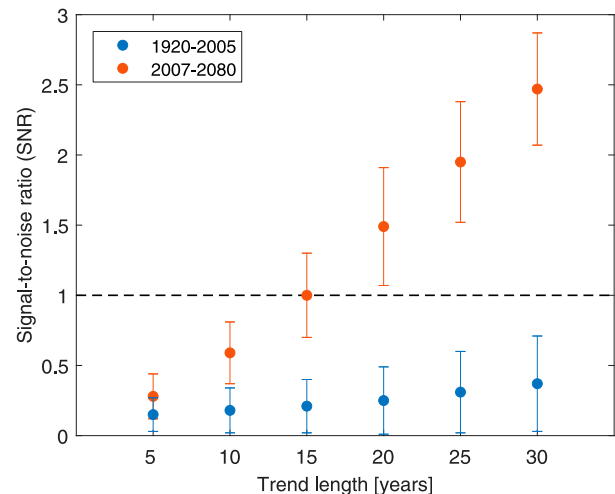

FIG. 6. Signal-to-noise ratio for Barents Sea ice extent trends as a function of trend length for the two time periods 1920–2005 and 2007–80. The SNR was calculated for all overlapping time intervals, and the figure shows the median values (markers) and interquartile spread (vertical bars). An SNR greater than one (values above the black dashed line) implies that the impact of the external forcing is stronger than the internal variability.
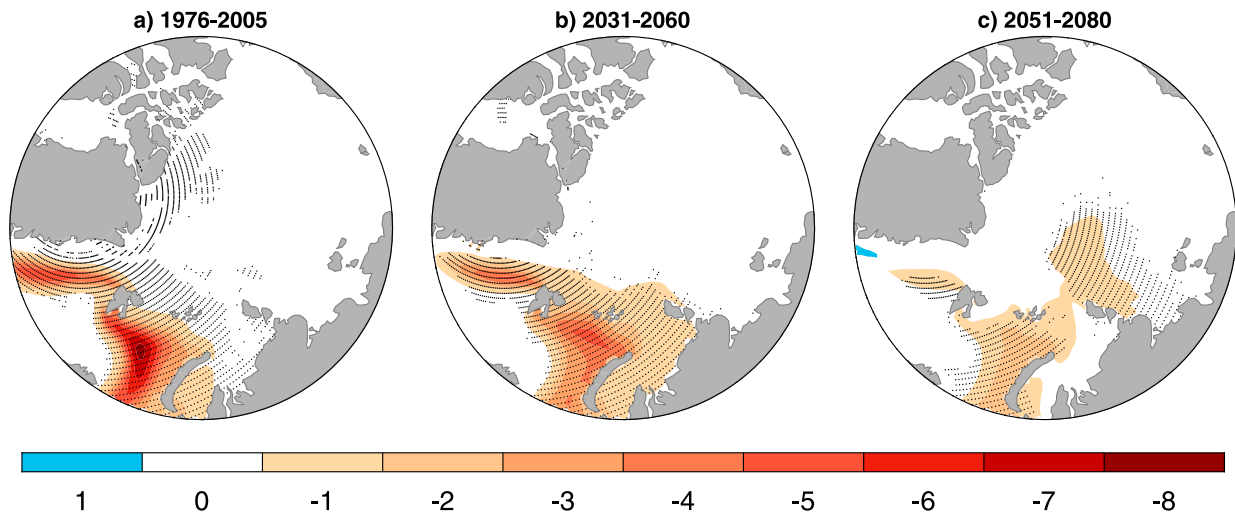
FIG. 7. The relationship between internally driven trends in BSO ocean heat transport and winter sea ice quantified by ensemble trend regressions, (a) for 1976–2005, (b) 2031–60, and (c) 2051–80. Regression coefficients have units of % per standard deviation of the ensemble spread in heat transport trends. Dots indicate where the ensemble trend correlation is significant at the 95% confidence level (Ebisuzaki 1997).

The results presented above (Figs. 3 and 8) are based on zero-lag correlations between OHT and wSIE. However, the correlation is also significant when OHT leads wSIE by one year ($r = -0.48$ averaged across the ensemble members). The former is consistent with spatially coherent wind-driven changes in Atlantic water heat transport that affect the sea ice cover immediately (Lien et al. 2017). The lagged response is, on the other hand, consistent with ocean heat anomalies advected through the Barents Sea with the mean flow, reaching the sea ice edge approximately one year after passing through the BSO (Årthun et al. 2012; Nakanowatari et al. 2014; Onarheim et al. 2015).

6. Drivers of future ocean heat transport variations

The future ensemble mean decline in Barents Sea wSIE corresponds to increased ocean heat transport through the BSO (Fig. 2), suggesting that OHT is also a key contributor to the externally forced decline in Barents Sea wSIE. This is further supported by the strong intermember correlation between future OHT and wSIE trends (r_{im}), especially for 2031–60 (Fig. 3). The ensemble mean increase in OHT toward year 2080 amounts to approximately 30 TW, corresponding to a 70% increase with respect to the historical mean (1920–2005). The future OHT increase in CESM-LE is a result of higher ocean temperature, counteracted by a decrease in the strength (volume) of the Atlantic inflow (Figs. 2c,d and 9). Conversely, heat transport covaries

with volume transport on interannual time scales; the multimember mean 30-yr (detrended) correlation being 0.91 (Fig. 9a). The correlation is also high for temperature (Fig. 9b). The relationship between OHT and ocean circulation strength thus differs for internal (interannual) and external (ensemble mean long-term trend) variability. We note that the strong interannual relationship between OHT and volume transport in CESM-LE is similar for previous decades (1976–2005), and agrees with observations (Årthun et al. 2012).

Several previous model studies have suggested that variations in AMOC are mirrored in OHT into the Arctic (e.g., Day et al. 2012; Zhang 2015; Delworth et al. 2016). We therefore assess to what extent the long-term weakening of the Barents Sea inflow (Fig. 2d) is related to ocean circulation changes in the North Atlantic. In CESM-LE, the AMOC substantially weakens toward 2080 (Fig. 10a) as a result of decreased buoyancy fluxes in the North Atlantic (Maroon et al. 2018). In contrast, however, the inflow to the Nordic Seas increases
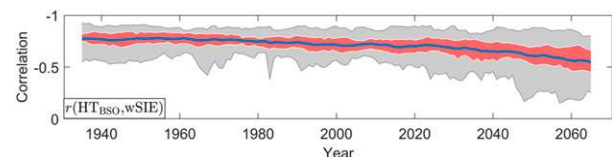

FIG. 8. Running 30-yr correlations between detrended winter Barents Sea ice extent (wSIE) and BSO heat transport (HT$_{BSO}$). The numbers are displayed at the center of each 30-yr period. Blue line: ensemble mean; red shading: interquartile range; gray shading: ensemble spread.
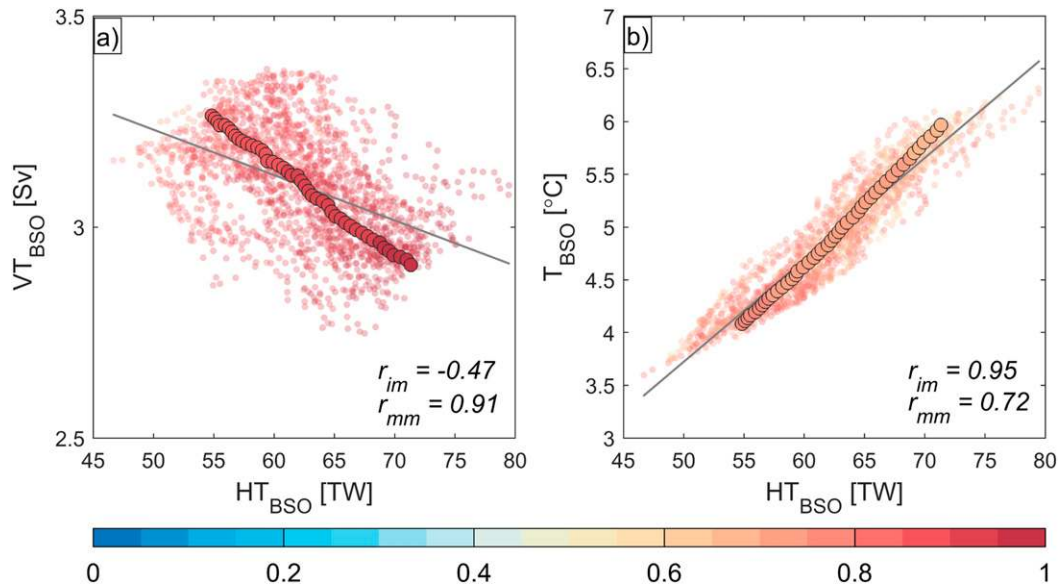
FIG. 9. The relationship between BSO heat transport (HT_{BSO}) and (a) volume transport (VT_{BSO}) and (b) temperature (T_{BSO}) for running 30-yr periods between 2007 and 2080 for all ensemble members (small circles). Colors show correlations for detrended time series. Multimember average correlation (r_{mm}) and intermember correlation (r_{im}) coefficients are provided. Linear regression lines are shown by solid lines. The larger circles show the correlation for each 30-yr period averaged over the ensemble members.

(Fig. 10d). The strengthened flow within the Nordic Seas is consistent with a trend toward lower sea level pressure (SLP) in the region (Fig. 11a), inducing a cyclonic circulation anomaly. The SLP decrease is, however, not spatially uniform, being larger in the northern BSO than in the south, which causes the SLP gradient across the Atlantic inflow to weaken (calculated as the difference between 74.5° and 71°N at 20°E). A weaker SLP and, hence, sea surface height gradient (not shown) across the BSO is associated with a weakened inflow (Ingvaldsen et al. 2004), consistent with Fig. 2d. The long-term (ensemble mean) decline in BSO is thus not directly related to a weaker AMOC, but rather to regional atmospheric circulation anomalies.

Internal AMOC variability is, on the other hand, related to changes in the inflow to the Barents Sea; a slowdown of the AMOC corresponds to weaker BSO transports (Figs. 10b,c). Note, however, that all 30-yr AMOC trends are negative, whereas the inflow to the Barents Sea has periods of both weakening and strengthening. Ocean circulation trends more immediately upstream in the Nordic Seas more strongly reflect inflow changes to the Barents Sea (Figs. 10e,f). In agreement with Oldenburg et al. (2018), these results suggest that the response in poleward ocean heat transport to changes in the AMOC differs under internal variability and climate change, with the relationship between AMOC trends and Nordic Seas

circulation changing sign depending on whether they are externally forced or a result of internal variability. Figure 10c furthermore shows that the influence of AMOC on the Barents Sea inflow weakens toward 2080. This is also true if we consider AMOC at 50°N. Ocean circulation (overturning) changes in the North Atlantic are thus to a lesser extent communicated toward the Arctic at the end of the century. The mechanisms of these future ocean circulation changes in the North Atlantic and Arctic, and their connectivity, are not assessed here and merit further study.

Internal variability in the atmosphere also influences the inflow to the Barents Sea. The ensemble trend regression between SLP and BSO volume transport yields a pattern that is dominated by low pressure over the central Arctic (Fig. 11b). The pattern is similar to the leading mode of Northern Hemisphere (>20°N) atmospheric circulation variability in CESM-LE, as inferred from an empirical orthogonal function analysis on wintertime SLP (not shown), and is reminiscent of the Arctic Oscillation (AO; Thompson and Wallace 1998). Trends in the associated principal component ("AO index") explain a significant fraction of the spread in BSO volume transport trends; the intermember correlation being 0.62 and 0.57 for 2031–50 and 2051–80, respectively. The importance of large-scale atmospheric circulation anomalies on Atlantic water transport into the Barents Sea is in agreement
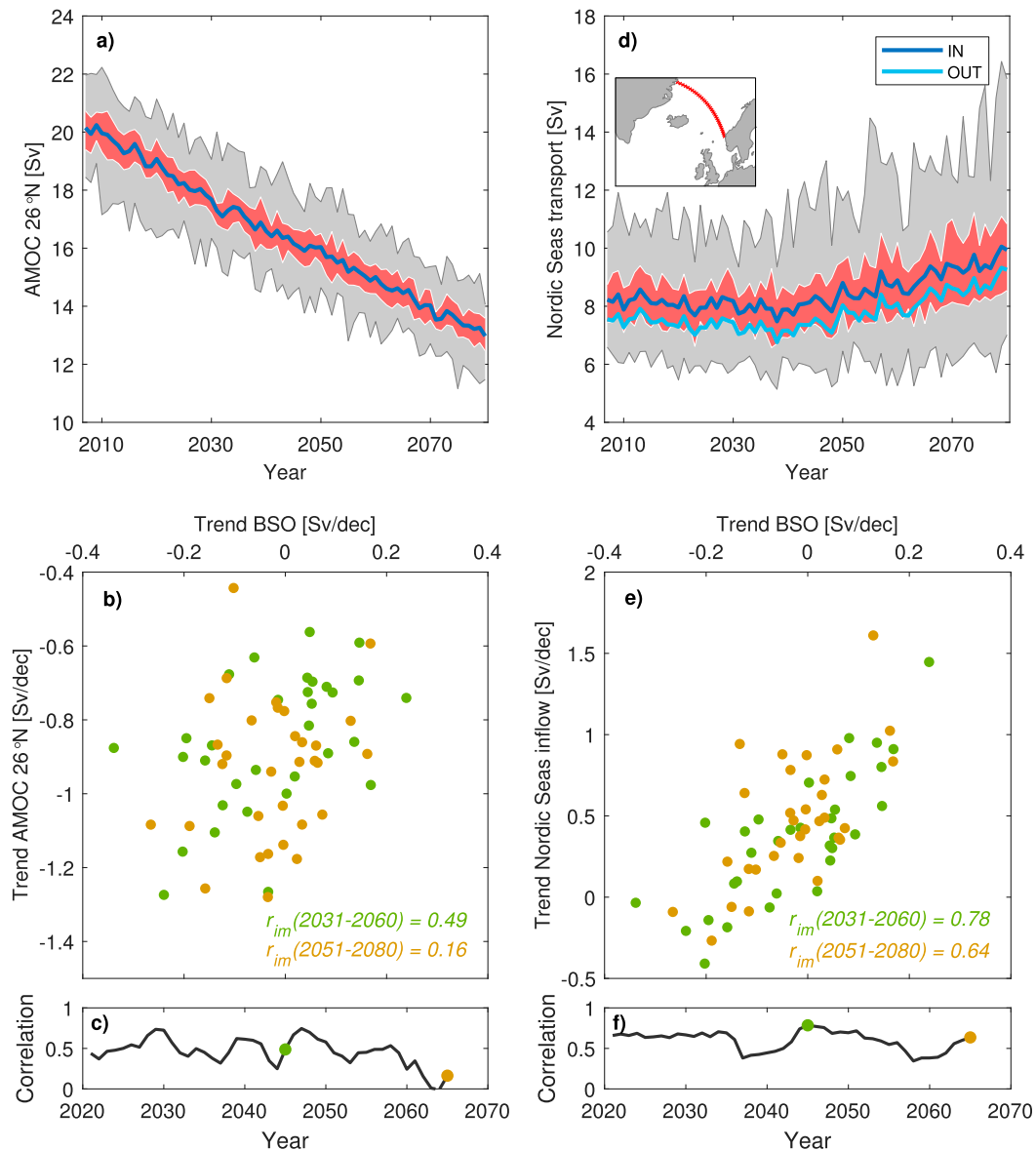
FIG. 10. North Atlantic–Arctic connectivity. (a) AMOC at 26°N. Blue line: ensemble mean; red shading: interquartile range; gray shading: ensemble spread. (b) The intermember relationship between 30-yr trends in AMOC and BSO volume transport for the time periods 2031–60 and 2051–80. (c) Running 30-yr intermember correlations between AMOC and BSO volume transport. The numbers are displayed at the center of each 30-yr period, and the two colored circles correspond to the two time periods shown in (b). (d)–(f) As in (a)–(c), but for the Nordic Seas inflow (section shown in inset map). In (d), the light blue line is the ensemble mean outflow.

with previous studies (e.g., Sandø et al. 2010; Smedsrud et al. 2013; Koenigk and Brodeau 2014).

7. Implications of future Atlantification of the Arctic

Water masses exported from the Barents Sea into the Arctic Ocean are important to the hydrographic structure of the central Arctic Ocean (Rudels et al. 2015). At present, most of the heat of the inflowing Atlantic water

masses through the BSO is lost to the atmosphere within the Barents Sea and the outflowing water thus provides little heat to the Eurasian basin (Gammelsrød et al. 2009; Årthun et al. 2011). However, as the temperature of the BSO inflow increases (Fig. 2c) the ensemble mean annual temperature of the water leaving the Barents Sea between Franz Josef Land and Novaya Zemlya (Barents Sea Exit; BSX) increases from −0.2° to 2.2°C between 2007 and 2080. The corresponding temperature difference
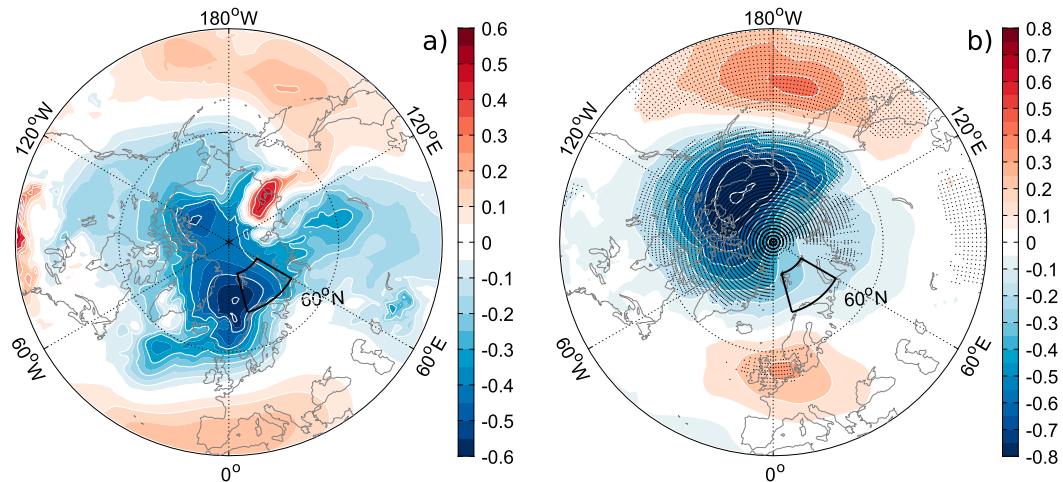
FIG. 11. (a) Linear trend in ensemble mean winter (November–April) sea level pressure (hPa decade^{-1}) for the time period 2007–80. The Barents Sea is highlighted by the black box. (b) The relationship between internally driven trends in BSO volume transport and winter sea level pressure between 2031 and 2060 quantified by ensemble trend regressions. Regression coefficients have units of hPa per standard deviation of the ensemble spread in volume transport trends. Dots indicate where the ensemble trend correlation is significant at the 95% confidence level (Ebisuzaki 1997).

between BSO and BSX nevertheless increases by approximately 0.6°C, pointing to a larger heat loss from the AW throughflow that mediates the Atlantic temperature increase. The increased heat loss amounts to 20 W m^{-2} for the Barents Sea as a whole. The additional heat loss is, however, the sum of different trends in the south and north. In the ice-free southern Barents Sea (70°–75°N, 15°–40°E) the ensemble mean total (sum of radiative and turbulent) surface heat loss is reduced from 200 to 170 W m^{-2} between 2007 and 2080. Conversely, in the northern Barents Sea (75°–81°N, 40°–60°E) the surface heat loss increases from 50 to 130 W m^{-2}.

The ability of a variable sea ice cover and associated surface heat fluxes to buffer the outflowing waters from changes in the inflowing Atlantic water is consistent with observations (Årthun et al. 2012; Smedsrud et al. 2013). The area over which Atlantic water cools, however, is set not only by the sea ice cover, but also by the location of the Polar Front (the boundary between Atlantic and Arctic waters in the eastern Barents Sea). Observations show that as the sea ice edge retreats northward, the northern limit of the surface area available for Atlantic water cooling becomes fixed to the location of the Polar Front (Barton et al. 2018). The buffering effect from a variable sea ice cover thus decreases, leading to a warming of the BSX outflow.

The future temperature increase in BSX is in agreement with Smedsrud et al. (2013) and Koenigk and Brodeau (2014), but in contrast to the findings of Long and Perrie (2017). Using a one-member simulation

forced with the SRES A1B climate change scenario Long and Perrie (2017) found temperatures in the northern Barents Sea to decrease toward 2050 as a result of increased surface heat loss. The different temperature response in previous studies could partly be a result of the different forcing scenarios (RCP8.5: strong; A1B: midrange, corresponding to RCP6.0), but it also highlights the possible influence of internally generated variability and the advantage of using a large ensemble simulation. However, with respect to the latter, no ensemble member in CESM-LE has a negative temperature trend in BSX for the time periods 2011–40, 2031–60, or 2051–80.

The ensemble mean temperature of the northward flowing Atlantic water in the eastern Fram Strait (79°N, 0°–12°E) shows a similar future increase to that in BSO; from 1.4°C in 2007 to 4.0°C in 2080. Although the Atlantic inflow through the Fram Strait is not discussed in detail here, the increased temperatures in this branch is consistent with reduced sea ice cover in the area north of Svalbard (Figs. 4 and 12b; Onarheim et al. 2014).

The warm Atlantic water gradually penetrates farther into the Arctic Ocean, and by the 2070s extends throughout the Eurasian basin (Fig. 12a). The poleward expansion of warmer water is associated with increased sea ice loss within the central Arctic (Fig. 4) and a northward migration of the sea ice edge (Fig. 12b). However, the sea ice edge does not retreat far beyond the northern Barents Sea by the 2070s. A reason for this is that the Atlantic heat enters the Eurasian basin as a subsurface flow and remains separated from the sea ice
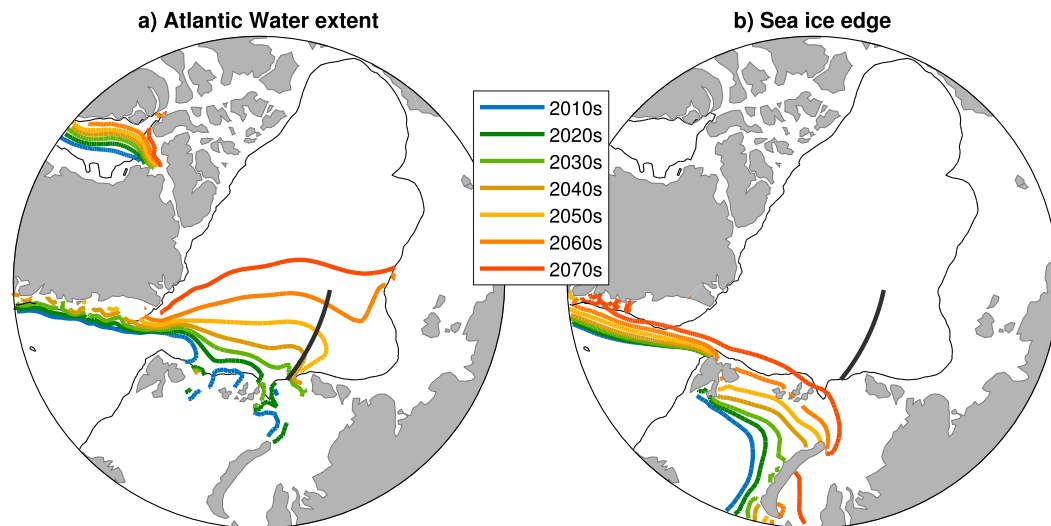
FIG. 12. Ensemble mean (a) Atlantic water extent represented by the 1°C isotherm at 200-m depth and (b) the winter sea ice edge (defined as 50% sea ice cover) for different decades between 2010 and 2079. The thin black lines show the 500-m isobath, which roughly marks the continental slopes, whereas the thick black line shows the section plotted in Fig. 13.

by a cold layer (Figs. 13a,b). The increase in Atlantic heat nevertheless has a noticeable influence on the winter sea ice thickness, evident by a 1.2-m average thickness reduction in the eastern Arctic Ocean between the 2010s and 2070s (Fig. 13c). The changes in sea ice thickness are associated with an increase in ocean-to-ice heat fluxes in this area from approximately $0.5\,\mathrm{W\,m^{-2}}$ in the 2010s to $5\,\mathrm{W\,m^{-2}}$ in the 2070s. The respective changes in winter ice thickness and ice–ocean heat fluxes are consistent with the inferred sensitivity of equilibrium ice thickness to changes in the different heat budget components by Thorndike (1992). The upward mixing of Atlantic heat within the Arctic Ocean, and its interaction with the sea ice cover, is, in nature, irregular both in time and space (e.g., Peterson et al. 2017), but this process is not detailed here. The decrease in sea ice thickness in CESM-LE is also evident in summer, and, consistent with a contribution from Atlantic heat transport, the thinning is seen to progress eastward from the Barents Sea (Labe et al. 2018).

8. Conclusions

In this study, the role of Atlantic heat transport in future Arctic winter sea ice loss is, for the first time, assessed using a 40-member large ensemble simulation (CESM-LE). We find the following:

1) Recent Arctic winter sea ice variability and trends (1976–2005) have largely been driven by internal variability. Externally forced variability becomes more important for multidecadal (>15 yr) sea ice trends in the future, whereas interannual to decadal

variability remains predominantly driven by internal variability. As a consequence, periods of increased sea ice cover, as observed during recent decades (Swart et al. 2015; Årthun et al. 2017), will likely still occur in the future when decadal internal variability counteracts anthropogenic forcing.

2) Ocean heat transport into the Barents Sea is, and will remain, a major source of internal Arctic sea ice variability during winter. The relationship between Atlantic heat transport and sea ice extent remains strong in the future, although weakening as the ice retreats. This implies that statistical prediction models based on observed relationships (e.g.,
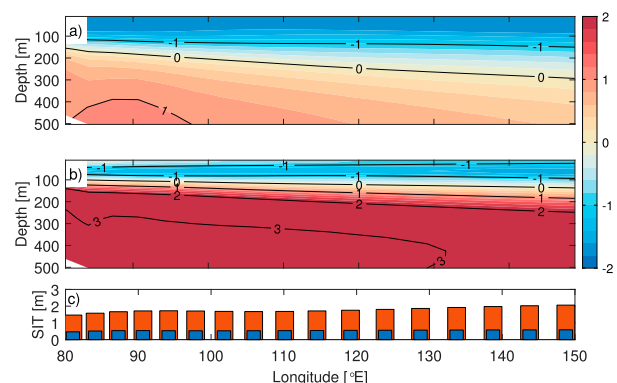

FIG. 13. (a),(b) Ensemble mean winter temperature (°C) during the recent decade (2010–19) and in the future (2070–79) in a section crossing the eastern Arctic Ocean (see location in Fig. 12). (c) Winter sea ice thickness (SIT) along the section for the two periods (2010–19: red; 2070–79: blue).

Onarheim et al. 2015) can also be expected to be skillful in the near future, but also highlights that the physical relationships that form the basis of statistical prediction models should continuously be reassessed.

3) The future ensemble-mean (externally forced) increase in ocean heat transport is a result of higher ocean temperatures, counteracted by a decrease in the strength of the flow. The reduced inflow to the Barents Sea results from regional atmospheric circulation trends, which change the relative strength of Atlantic water pathways into the Arctic. The circulation within the Nordic Seas is strengthened in the future, in contrast to a slowdown of the large-scale circulation in the North Atlantic, as represented by the AMOC. Internally driven increases (decreases) in heat transport into the Barents Sea are, on the other hand, associated with a strengthening (weakening) of the flow, related to upstream ocean circulation changes in the North Atlantic and Nordic Seas, and large-scale atmospheric circulation anomalies reminiscent of the Arctic Oscillation.

4) The future increase in Atlantic heat transport is reflected in a northward penetration of warm water into the Arctic Ocean, which contributes to a substantial reduction in sea ice thickness.

Although the CESM-LE represents well present-day ice–ocean interaction in the Barents Sea (section 3), it is important to keep in mind that future simulations are inherently uncertain. In particular, upper-ocean stratification and vertical mixing (Carmack et al. 2015; Lind et al. 2018), which affects the transfer of oceanic heat to the overlying sea ice cover, are difficult to correctly represent in coarse-resolution climate models (Ilıcak et al. 2016; Lique et al. 2016). This could influence how the simulated future increase in Atlantic heat impacts the Arctic sea ice. Compared with present-day observations, CESM has a cold temperature bias and an overestimated sea ice cover (Fig. 2a; Park et al. 2014). The response in sea ice extent to changes in ocean heat transport is nevertheless realistic (section 3). This suggests that the simulated "Atlantification" of the Arctic Ocean and associated impacts can be considered realistic, but—as the Atlantic domain evolves from farther south than in reality—the simulated development could be delayed. The observed trend in winter Barents Sea ice extent during recent decades is larger than in any of the CESM ensemble members (Onarheim and Årthun 2017), and the current winter sea ice extent is at least 20 years ahead of any ensemble member (Fig. 2a).

Our results demonstrate that Atlantic heat transport plays an important role in recent and future Arctic winter sea ice variability and trends. As a warmer and ice-free Arctic Ocean could have profound consequences for the Arctic climate system (Vihma 2014; Carmack et al. 2015), it is important to identify the main drivers of sea ice variability and retreat. A better understanding of the relative roles of internal and external variability in Arctic winter sea ice variability and trends on different time scales, as provided here, is also essential in order to skillfully predict future sea ice changes under anthropogenic warming.

REFERENCES

Arrigo, K. R., and G. L. van Dijken, 2011: Secular trends in Arctic Ocean net primary production. *J. Geophys. Res.*, **116**, C09011, https://doi.org/10.1029/2011JC007151.

Årthun, M., R. Ingvaldsen, L. H. Smedsrud, and C. Schrum, 2011: Dense water formation and circulation in the Barents Sea. *Deep-Sea Res.*, **58**, 801–817, https://doi.org/10.1016/j.dsr.2011.06.001.

——, T. Eldevik, L. H. Smedsrud, Ø. Skagseth, and R. B. Ingvaldsen, 2012: Quantifying the influence of Atlantic heat on Barents Sea ice variability and retreat. *J. Climate*, **25**, 4736–4743, https://doi.org/10.1175/JCLI-D-11-00466.1.

——, ——, E. Viste, H. Drange, T. Furevik, H. L. Johnson, and N. S. Keenlyside, 2017: Skillful prediction of northern climate provided by the ocean. *Nat. Commun.*, **8**, 15875, https://doi.org/10.1038/ncomms15875.

——, B. Bogstad, U. Daewel, N. Keenlyside, A. Sandø, C. Schrum, and G. Ottersen, 2018: Climate based multi-year predictions of the Barents Sea cod stock. *PLOS ONE*, **13**, e0206319, https://doi.org/10.1371/journal.pone.0206319.

Barnhart, K. R., C. R. Miller, I. Overeem, and J. E. Kay, 2016: Mapping the future expansion of Arctic open water. *Nat. Climate Change*, **6**, 280–285, https://doi.org/10.1038/nclimate2848.

Barton, B. I., Y.-D. Lenn, and C. Lique, 2018: Observed Atlantification of the Barents Sea causes the polar front to limit the expansion of winter sea ice. *J. Phys. Oceanogr.*, **48**, 1849–1866, https://doi.org/10.1175/JPO-D-18-0003.1.

Beszczynska-Möller, A., R. Woodgate, C. Lee, H. Melling, and M. Karcher, 2011: A synthesis of exchanges through the main oceanic gateways to the Arctic Ocean. *Oceanography*, **24**, 82–99, https://doi.org/10.5670/oceanog.2011.59.

Bhatt, U. S., and Coauthors, 2014: Implications of Arctic sea ice decline for the Earth system. *Annu. Rev. Environ. Resour.*, **39**, 57–89, https://doi.org/10.1146/annurev-environ-122012-094357.

Carmack, E., and Coauthors, 2015: Toward quantifying the increasing role of oceanic heat in sea ice loss in the new Arctic. *Bull. Amer. Meteor. Soc.*, **96**, 2079–2105, https://doi.org/10.1175/BAMS-D-13-00177.1.

Cavalieri, D. J., and C. L. Parkinson, 2012: Arctic sea ice variability and trends, 1979–2010. *Cryosphere*, **6**, 881–889, https://doi.org/10.5194/tc-6-881-2012.

Day, J., J. Hargreaves, J. Annan, and A. Abe-Ouchi, 2012: Sources of multi-decadal variability in Arctic sea ice extent. *Environ. Res. Lett.*, **7**, 034011, https://doi.org/10.1088/1748-9326/7/3/034011.

Delworth, T. L., F. Zeng, G. A. Vecchi, X. Yang, L. Zhang, and R. Zhang, 2016: The North Atlantic Oscillation as a driver of rapid climate change in the Northern Hemisphere. *Nat. Geosci.*, **9**, 509–512, https://doi.org/10.1038/ngeo2738.

Deser, C., A. S. Phillips, M. A. Alexander, and B. V. Smoliak, 2014: Projecting North American climate over the next 50 years: Uncertainty due to internal variability. *J. Climate*, **27**, 2271–2296, https://doi.org/10.1175/JCLI-D-13-00451.1.

Ding, Q., and Coauthors, 2017: Influence of high-latitude atmospheric circulation changes on summertime Arctic sea ice. *Nat. Climate Change*, **7**, 289–295, https://doi.org/10.1038/nclimate3241.

Ebisuzaki, W., 1997: A method to estimate the statistical significance of a correlation when the data are serially correlated. *J. Climate*, **10**, 2147–2153, https://doi.org/10.1175/1520-0442(1997)010<2147:AMTETS>2.0.CO;2.

Francis, J. A., and E. Hunter, 2007: Drivers of declining sea ice in the Arctic winter: A tale of two seas. *Geophys. Res. Lett.*, **34**, L17503, https://doi.org/10.1029/2007GL030995.

Gammelsrød, T., Ø. Leikvin, V. Lien, W. P. Budgell, H. Loeng, and W. Maslowski, 2009: Mass and heat transports in the NE Barents Sea: Observations and models. *J. Mar. Syst.*, **75**, 56–69, https://doi.org/10.1016/j.jmarsys.2008.07.010.

Hodson, D. L., S. P. Keeley, A. West, J. Ridley, E. Hawkins, and H. T. Hewitt, 2013: Identifying uncertainties in Arctic climate change projections. *Climate Dyn.*, **40**, 2849–2865, https://doi.org/10.1007/s00382-012-1512-z.

Holland, M. M., and J. Stroeve, 2011: Changing seasonal sea ice predictor relationships in a changing Arctic climate. *Geophys. Res. Lett.*, **38**, L18501, https://doi.org/10.1029/2011GL049303.

——, C. M. Bitz, and B. Tremblay, 2006: Future abrupt reductions in the summer Arctic sea ice. *Geophys. Res. Lett.*, **33**, L23503, https://doi.org/10.1029/2006GL028024.

——, D. A. Bailey, and S. Vavrus, 2011: Inherent sea ice predictability in the rapidly changing Arctic environment of the Community Climate System Model, version 3. *Climate Dyn.*, **36**, 1239–1253, https://doi.org/10.1007/s00382-010-0792-4.

Hurrell, J. W., and Coauthors, 2013: The Community Earth System Model: A framework for collaborative research. *Bull. Amer. Meteor. Soc.*, **94**, 1339–1360, https://doi.org/10.1175/BAMS-D-12-00121.1.

Ilıcak, M., and Coauthors, 2016: An assessment of the Arctic Ocean in a suite of interannual CORE-II simulations. Part III: Hydrography and fluxes. *Ocean Modell.*, **100**, 141–161, https://doi.org/10.1016/j.ocemod.2016.02.004.

Ingvaldsen, R. B., L. Asplin, and H. Loeng, 2004: Velocity field of the western entrance to the Barents Sea. *J. Geophys. Res.*, **109**, C03021, https://doi.org/10.1029/2003JC001811.

Jahn, A., J. E. Kay, M. M. Holland, and D. M. Hall, 2016: How predictable is the timing of a summer ice-free Arctic? *Geophys. Res. Lett.*, **43**, 9113–9120, https://doi.org/10.1002/2016GL070067.

Kay, J. E., M. M. Holland, and A. Jahn, 2011: Inter-annual to multi-decadal Arctic sea ice extent trends in a warming world. *Geophys. Res. Lett.*, **38**, L15708, https://doi.org/10.1029/2011GL048008.

——, and Coauthors, 2015: The Community Earth System Model (CESM) large ensemble project: A community resource for studying climate change in the presence of internal climate variability. *Bull. Amer. Meteor. Soc.*, **96**, 1333–1349, https://doi.org/10.1175/BAMS-D-13-00255.1.

Kim, W. M., S. Yeager, P. Chang, and G. Danabasoglu, 2018: Low-frequency North Atlantic climate variability in the Community Earth System Model Large Ensemble. *J. Climate*, **31**, 787–813, https://doi.org/10.1175/JCLI-D-17-0193.1.

Koenigk, T., and L. Brodeau, 2014: Ocean heat transport into the Arctic in the twentieth and twenty-first century in EC-Earth. *Climate Dyn.*, **42**, 3101–3120, https://doi.org/10.1007/s00382-013-1821-x.

Kovacs, K. M., C. Lydersen, J. E. Overland, and S. E. Moore, 2011: Impacts of changing sea-ice conditions on Arctic marine mammals. *Mar. Biodiversity*, **41**, 181–194, https://doi.org/10.1007/s12526-010-0061-0.

Krishfield, R. A., A. Proshutinsky, K. Tateyama, W. J. Williams, E. C. Carmack, F. A. McLaughlin, and M.-L. Timmermans, 2014: Deterioration of perennial sea ice in the Beaufort Gyre from 2003 to 2012 and its impact on the oceanic freshwater cycle. *J. Geophys. Res.*, **119**, 1271–1305, https://doi.org/10.1002/2013JC008999.

Labe, Z., G. Magnusdottir, and H. Stern, 2018: Variability of Arctic sea ice thickness using PIOMAS and the CESM Large Ensemble. *J. Climate*, **31**, 3233–3247, https://doi.org/10.1175/JCLI-D-17-0436.1.

Lee, S., T. Gong, S. B. Feldstein, J. A. Screen, and I. Simmonds, 2017: Revisiting the cause of the 1989–2009 Arctic surface warming using the surface energy budget: Downward infrared radiation dominates the surface fluxes. *Geophys. Res. Lett.*, **44**, 10 654–10 661, https://doi.org/10.1002/2017GL075375.

Li, D., R. Zhang, and T. R. Knutson, 2017: On the discrepancy between observed and CMIP5 multi-model simulated Barents Sea winter sea ice decline. *Nat. Commun.*, **8**, 14991, https://doi.org/10.1038/ncomms14991.

Lien, V. S., P. Schlichtholz, Ø. Skagseth, and F. B. Vikebø, 2017: Wind-driven Atlantic water flow as a direct mode for reduced Barents Sea ice cover. *J. Climate*, **30**, 803–812, https://doi.org/10.1175/JCLI-D-16-0025.1.

Lind, S., R. B. Ingvaldsen, and T. Furevik, 2018: Arctic warming hotspot in the northern Barents Sea linked to declining sea-ice import. *Nat. Climate Change*, **8**, 634–639, https://doi.org/10.1038/s41558-018-0205-y.

Lique, C., M. M. Holland, Y. B. Dibike, D. M. Lawrence, and J. A. Screen, 2016: Modeling the Arctic freshwater system and its integration in the global system: Lessons learned and future challenges. *J. Geophys. Res.*, **121**, 540–566, https://doi.org/10.1002/2015JG003120.

Long, Z., and W. Perrie, 2017: Changes in ocean temperature in the Barents Sea in the twenty-first century. *J. Climate*, **30**, 5901–5921, https://doi.org/10.1175/JCLI-D-16-0415.1.

Maroon, E. A., J. E. Kay, and K. B. Karnauskas, 2018: Influence of the Atlantic meridional overturning circulation on the Northern Hemisphere surface temperature response to radiative forcing. *J. Climate*, **31**, 9207–9224, https://doi.org/10.1175/JCLI-D-17-0900.1.

Nakanowatari, T., K. Sato, and J. Inoue, 2014: Predictability of the Barents Sea ice in early winter: Remote effects of oceanic and atmospheric thermal conditions from the North Atlantic. *J. Climate*, **27**, 8884–8901, https://doi.org/10.1175/JCLI-D-14-00125.1.

Ogawa, F., and Coauthors, 2018: Evaluating impacts of recent Arctic sea ice loss on the Northern Hemisphere winter climate change. *Geophys. Res. Lett.*, **45**, 3255–3263, https://doi.org/10.1002/2017GL076502.

Oldenburg, D., K. C. Armour, L. Thompson, and C. M. Bitz, 2018: Distinct mechanisms of ocean heat transport into the Arctic under internal variability and climate change. *Geophys. Res. Lett.*, **45**, 7692–7700, https://doi.org/10.1029/2018GL078719.

Onarheim, I. H., and M. Årthun, 2017: Toward an ice-free Barents Sea. *Geophys. Res. Lett.*, **44**, 8387–8395, https://doi.org/10.1002/2017GL074304.

——, L. H. Smedsrud, R. B. Ingvaldsen, and F. Nilsen, 2014: Loss of sea ice during winter north of Svalbard. *Tellus*, **66A**, 23933, https://doi.org/10.3402/tellusa.v66.23933.

——, T. Eldevik, M. Årthun, R. B. Ingvaldsen, and L. H. Smedsrud, 2015: Skillful prediction of Barents Sea ice cover. *Geophys. Res. Lett.*, **42**, 5364–5371, https://doi.org/10.1002/2015GL064359.

——, ——, L. H. Smedsrud, and J. C. Stroeve, 2018: Seasonal and regional manifestation of Arctic sea ice loss. *J. Climate*, **31**, 4917–4932, https://doi.org/10.1175/JCLI-D-17-0427.1.

Overland, J. E., and M. Wang, 2007: Future regional Arctic sea ice declines. *Geophys. Res. Lett.*, **34**, L17705, https://doi.org/10.1029/2007GL030808.

Park, T.-W., Y. Deng, M. Cai, J.-H. Jeong, and R. Zhou, 2014: A dissection of the surface temperature biases in the Community Earth System Model. *Climate Dyn.*, **43**, 2043–2059, https://doi.org/10.1007/s00382-013-2029-9.

Peterson, A. K., I. Fer, M. G. McPhee, and A. Randelhoff, 2017: Turbulent heat and momentum fluxes in the upper ocean under Arctic sea ice. *J. Geophys. Res.*, **122**, 1439–1456, https://doi.org/10.1002/2016JC012283.

Polyakov, I. V., and Coauthors, 2017: Greater role for Atlantic inflows on sea-ice loss in the Eurasian Basin of the Arctic Ocean. *Science*, **356**, 285–291, https://doi.org/10.1126/science.aai8204.

Rayner, N., D. E. Parker, E. Horton, C. Folland, L. Alexander, D. Rowell, E. Kent, and A. Kaplan, 2003: Global analyses of sea surface temperature, sea ice, and night marine air temperature since the late nineteenth century. *J. Geophys. Res.*, **108**, 4407, https://doi.org/10.1029/2002JD002670.

Rudels, B., M. Korhonen, U. Schauer, S. Pisarev, B. Rabe, and A. Wisotzki, 2015: Circulation and transformation of Atlantic water in the Eurasian Basin and the contribution of the Fram Strait inflow branch to the Arctic Ocean heat budget. *Prog. Oceanogr.*, **132**, 128–152, https://doi.org/10.1016/j.pocean.2014.04.003.

Sandø, A. B., J. Nilsen, Y. Gao, and K. Lohmann, 2010: Importance of heat transport and local air-sea heat fluxes for Barents Sea climate variability. *J. Geophys. Res.*, **115**, C07013, https://doi.org/10.1029/2009JC005884.

——, A. Melsom, and W. P. Budgell, 2014: Downscaling IPCC control run and future scenario with focus on the Barents Sea. *Ocean Dyn.*, **64**, 927–949, https://doi.org/10.1007/s10236-014-0731-8.

Schauer, U., and A. Beszczynska-Möller, 2009: Problems with estimation and interpretation of oceanic heat transport–conceptual remarks for the case of Fram Strait in the Arctic Ocean. *Ocean Sci.*, **5**, 487–494, https://doi.org/10.5194/os-5-487-2009.

Screen, J. A., 2017: Simulated atmospheric response to regional and pan-Arctic sea ice loss. *J. Climate*, **30**, 3945–3962, https://doi.org/10.1175/JCLI-D-16-0197.1.

Serreze, M. C., and J. Stroeve, 2015: Arctic sea ice trends, variability and implications for seasonal ice forecasting. *Philos. Trans. Roy. Soc.*, **373A**, 20140159, https://doi.org/10.1098/rsta.2014.0159.

——, M. M. Holland, and J. Stroeve, 2007: Perspectives on the Arctic's shrinking sea-ice cover. *Science*, **315**, 1533–1536, https://doi.org/10.1126/science.1139426.

Sévellec, F., A. V. Fedorov, and W. Liu, 2017: Arctic sea-ice decline weakens the Atlantic meridional overturning circulation. *Nat. Climate Change*, **7**, 604–610, https://doi.org/10.1038/nclimate3353.

Smedsrud, L. H., and Coauthors, 2013: The role of the Barents Sea in the Arctic climate system. *Rev. Geophys.*, **51**, 415–449, https://doi.org/10.1002/rog.20017.

Stroeve, J. C., M. C. Serreze, M. M. Holland, J. E. Kay, J. Malanik, and A. P. Barrett, 2012: The Arctic's rapidly shrinking sea ice cover: A research synthesis. *Climatic Change*, **110**, 1005–1027, https://doi.org/10.1007/s10584-011-0101-1.

Swart, N. C., J. C. Fyfe, E. Hawkins, J. E. Kay, and A. Jahn, 2015: Influence of internal variability on Arctic sea-ice trends. *Nat. Climate Change*, **5**, 86–89, https://doi.org/10.1038/nclimate2483.

Taylor, K. E., R. J. Stouffer, and G. A. Meehl, 2012: An overview of CMIP5 and the experiment design. *Bull. Amer. Meteor. Soc.*, **93**, 485–498, https://doi.org/10.1175/BAMS-D-11-00094.1.

Thompson, D. W., and J. M. Wallace, 1998: The Arctic Oscillation signature in the wintertime geopotential height and temperature fields. *Geophys. Res. Lett.*, **25**, 1297–1300, https://doi.org/10.1029/98GL00950.

Thorndike, A., 1992: A toy model linking atmospheric thermal radiation and sea ice growth. *J. Geophys. Res.*, **97**, 9401–9410, https://doi.org/10.1029/92JC00695.

Tietsche, S., D. Notz, J. H. Jungclaus, and J. Marotzke, 2013: Predictability of large interannual Arctic sea-ice anomalies. *Climate Dyn.*, **41**, 2511–2526, https://doi.org/10.1007/s00382-013-1698-8.

Vihma, T., 2014: Effects of Arctic sea ice decline on weather and climate: A review. *Surv. Geophys.*, **35**, 1175–1214, https://doi.org/10.1007/s10712-014-9284-0.

Walsh, J. E., F. Fetterer, J. S. Stewart, and W. L. Chapman, 2017: A database for depicting Arctic sea ice variations back to 1850. *Geogr. Rev.*, **107**, 89–107, https://doi.org/10.1111/j.1931-0846.2016.12195.x.

Wettstein, J. J., and C. Deser, 2014: Internal variability in projections of twenty-first-century Arctic sea ice loss: Role of the large-scale atmospheric circulation. *J. Climate*, **27**, 527–550, https://doi.org/10.1175/JCLI-D-12-00839.1.

Yeager, S. G., A. R. Karspeck, and G. Danabasoglu, 2015: Predicted slowdown in the rate of Atlantic sea ice loss. *Geophys. Res. Lett.*, **42**, 10 704–10 713, https://doi.org/10.1002/2015GL065364.

Zhang, R., 2015: Mechanisms for low-frequency variability of summer Arctic sea ice extent. *Proc. Natl. Acad. Sci. USA*, **112**, 4570–4575, https://doi.org/10.1073/pnas.1422296112.